# Neutron scattering study of nitrogen adsorbed on basal-plane-oriented graphite*

J. K. Kjems,† L. Passell, and H. Taub
*Brookhaven National Laboratory, Upton, New York 11973*

J. G. Dash
*University of Washington, Seattle, Washington 98195*

A. D. Novaco
*Lafayette College, Easton, Pennsylvania 18042*

(Received 6 August 1975)

Thermal-neutron scattering has been used to investigate the structure of nitrogen films adsorbed on Grafoil, a basal-plane-oriented graphite. Diffraction scans were made at coverages between 1/3 of a monolayer and 7/4 monolayers over a temperature range from 10 to 90 K. The observed line shapes were analyzed and found to be generally consistent with the predictions of two-dimensional diffraction theory. From the data at least three distinct surface phases can be identified: (i) a low-temperature epitaxial phase with a triangular lattice structure, (ii) a more compressed low-temperature phase with the same structure but not in registry with the substrate, and (iii) one or more high-temperature disordered phases. Changes in the slope of the adsorption isotherm are found to correlate well with the observed transitions from one phase to another.

## I. INTRODUCTION

It has recently been discovered that physisorbed gas films can form states of a unique, two-dimension (2D)-like character.[1] Evidence for this comes primarily from investigations of the vapor-pressure isotherms and heat capacities of monolayer films deposited on a special group of substrates, materials such as graphitized carbon black,[2,3] cube crystals of alkali halides,[4,5] vapor-deposited crystals of layer compounds such as $FeCl_2$,[6] exfoliated graphite,[7] and a related product, partially oriented graphite foil,[8,9] known commerically as Grafoil.[10] All are substances which can be prepared with surfaces uniform enough to reveal the behavior of the film without obscuring effects due to defects and impurities.

Experiments on uniform surfaces have produced some striking results. For instance, on single crystals of graphite, adsorption isotherms show sharply defined "stair-step" patterns indicative of a discrete, layer-by-layer condensing process. Studies of the heat capacities of adsorbed phases[9,11] have also been very revealing. These show not only indications of phase transitions analogous to the vapor-liquid-solid transitions of 3D matter but also evidence of structural rearrangements of the kind associated with transitions from one ordered phase to another.[8,9,12–14]

Ultimately, the aim of such experiments is to relate the observed macroscopic properties of adsorbed phases to the interactions of atoms on surfaces—a goal which is closely tied to the availability of realistic microscopic models of surfaces and surface films. Thus further improvement in our understanding of surface interactions depends crucially on expanding our knowledge of *microscopic* surface phenomena. Fortunately, methods for probing surfaces on an atomic scale have been under intensive development and are now beginning to supply the necessary information.

The first microscopic measurements on adsorbed phases were reported in 1967 by Lander and Morrison[15] who used low-energy-electron diffraction (LEED) to study a number of gases deposited on single-crystal graphite surfaces. One weakly physisorbed gas, xenon, was examined. This, they found, formed an ordered $\sqrt{3}\times\sqrt{3}$ epitaxial layer on the graphite basal planes at temperatures below 90 K. Later the Xe-graphite system was studied under somewhat better defined conditions of temperature and pressure by Suzanne, Coulomb, and Bienfait[16] using both LEED and Auger spectroscopy. Other LEED investigations of physisorbed films have been reported by Palmberg,[17] who studied Xe on (100) faces of Pd, and by Farrell, Strongin, and Dickey,[18] who examined Ne, Ar, Kr, and Xe adsorbed on (100) faces of Nb. In all cases there were indications of the formation of epitaxial structures although in the case of Xe on Pd ordering was only observed near monolayer coverage.

On surface films more loosely bound than Xe, LEED measurements have not been very informative. The trouble stems primarily from the fact that these films are rapidly desorbed by the incident electron beam.[18] Indeed, there is reason to believe that desorption difficulties plus the need for high vacuum above the substrate surface will probably limit LEED to studies of chemisorbed phases and the more firmly bound physisorbed

systems. For the same reasons, it also seems clear that other charged-particle-beam methods[19,20] are unlikely to be of wider application.

We have recently begun exploring the use of neutron scattering as an alternative microscopic probe of adsorbed phases. Experience to date indicates that although this technique is more limited than LEED in the number of systems to which it can be applied it has compensating advantages. These include the fact that desorption is not a problem nor is the presence of vapor above the sample surface. Thus, when neutrons can be used, a broad range of film coverages and temperatures becomes accessible to investigation.

An additional attraction of the neutron method is that it provides a direct approach to microscopic film dynamics although intensity problems will probably limit practical applications in this area to a few special cases. In this paper we will not make any attempt to discuss the application of *inelastic* neutron scattering methods to the study of surface film dynamics. Nevertheless it might be of interest to mention that we are currently investigating the inelastic scattering from $^{36}Ar$ adsorbed on Grafoil and that some results relating to the dynamic behavior of argon monolayers have already been published.[21]

Our first experiments involving nitrogen adsorbed on Grafoil have already been briefly reported.[22] Here we would like to expand on the general application of neutrons to surface-film studies and to describe in detail how our $N_2$ measurements were made and the data analyzed. We would also like to present additional $N_2$ data representing a wider range of film coverages and temperatures and to offer our views as to how such data can be interpreted in microscopic terms.

The text is organized as follows: In Sec. II we discuss the application of neutron diffraction to the study of surface films and compare neutrons with electrons as surface probes. Section III contains a brief description of the experimental apparatus. In Sec. IV we consider how the 2D-like character of the films influences the scattering and how the observed diffraction patterns can be used to derive information concerning the structures of films and substrates. Our experimental data are presented in Sec. V and their analysis in Sec. VI. Finally, Sec. VII is devoted to a discussion of the conclusions which we believe can be drawn from these investigations.

## II. APPLICATION OF NEUTRON SCATTERING TO ADSORBED FILM STUDIES

Slow neutron scattering is widely used as a microscopic probe of condensed matter. As is well known, both elastic and inelastic methods are employed, the former for structural studies and the latter for investigations of excitation spectra. For applications to 2D-like surface films, the techniques are only marginally different from those used for more conventional 3D studies. About the only important difference is that background scattering (from the substrate) is more of a problem. This difficulty arises because neutrons, unlike charges particles, are weakly interacting probes and therefore penetrate almost uniformly through the sample volume. Since neutrons do not preferentially interact at surfaces, scattering from surface films will ordinarily not be distinguishable from scattering by the substrate. Only in special cases is the scattering from surface layers readily identified. These occur when gases which are reasonably intense scatterers of neutrons are deposited on relatively transparent substrates of large specific area.

To give an idea of which gases are useful in this circumstance we have compiled in Table I the neutron scattering and capture cross sections of a selection of gases commonly employed for physisorption investigations.[23] Since the atoms and molecules listed are of roughly the same size, the monolayer capacity of a given substrate will be approximately the same for all of these gases. Consequently, except for losses due to neutron capture, the diffracted intensities at monolayer coverages can be expected to be more or less proportional to the listed cross sections. Inspection of the table shows immediately that $N_2$ and the separated isotope $^{36}Ar$ are the most attractive candidates for neutron studies.

TABLE I. Neutron scattering and capture cross sections of some gases commonly used for physisorption studies.

| Gas | $4\pi(\sum_j b_j)^2$ [a] (b) | $l$ [b] (Å) | $4\pi(\sum_j b_j)^2 j_0(\frac{1}{2}Ql)^2$ [c] (b) | $\sigma_a$ [d] (b) |
|---|---|---|---|---|
| $^4He$ | 1.13 | | 1.13 | ... |
| Ne | 2.66 | | 2.66 | 0.032 |
| $^{36}Ar$ | 74.20 | | 74.20 | 0.005 |
| Kr | 6.88 | | 6.88 | 25.0 |
| Xe | 2.90 | | 2.90 | 24.5 |
| $H_2$ | 7.03 | 0.742 | 6.13 | 0.66 |
| $D_2$ | 22.36 | 0.742 | 19.49 | 0.001 |
| $N_2$ | 44.41 | 1.094 | 32.75 | 3.7 |
| $O_2$ | 16.90 | 1.207 | 11.64 | 0.001 |
| $Cl_2$ | 46.13 | 1.988 | 15.47 | 66.0 |

[a]Coherent scattering amplitudes of bound atoms from C. G. Shull (private communication).

[b]Bond lengths from G. Herzberg, *Molecular Spectra and Molecular Structure, I Spectra of Diatomic molecules*, 2nd ed. (Van Nostrand, New York, 1950).

[c]Scattering cross section evaluated at $Q = 1.71$ Å$^{-1}$, the wave vector corresponding to the diffraction peak for the $\sqrt{3}\times\sqrt{3}$ registered phase on graphite.

[d]Capture cross section at $E_n = 0.0253$ eV.

As we mentioned, apart from choosing a gas which is an intense scatterer of neutrons, the other essential for neutron experiments on surface films is relative transparency of the substrate. Clearly this requires the selection of substrates with small scattering and capture cross sections. But sometimes an additional factor can be brought into play to improve transparency. Adsorbed films quite commonly have more open structures than the substrates on which they are deposited. In this circumstance it is often possible to choose a neutron wavelength which is large enough to be near or even beyond the crystalline cutoff for Bragg scattering from the substrate but is at the same time not too large for Bragg scattering from the surface layer. Thus background scattering from the substrate can be substantially reduced or even eliminated while diffraction from the film is little affected. This technique will, of course, only be applicable when interatomic distances in the surface layer are significantly larger than those in the substrate.

Another helpful feature for improving contrast between scattering from film and substrate is preferred orientation in the substrate. The reasons for this will be discussed in detail in Sec. IV. And, while unrelated to the gain in contrast, preferred orientation can also be helpful because it permits selective study of scattering in and normal to the adsorbed film plane. This is a particularly valuable feature in inelastic experiments.

Finally, while still on the subject of contrast, it should be noted that since the intensity of scattering from the surface film compared to the background of scattering from the substrate depends directly on the relative numbers of adsorbate and adsorber atoms, it is essential for neutron scattering to have substrates with very large surface areas.

Remarkably, Grafoil—a commonly employed adsorber for macroscopic experiments—is also an excellent material for neutron investigations. In part this is because carbon has a moderate sized scattering and very small capture cross section. Of more importance, however, is the very large specific area of predominantly basal plane surface Grafoil and its preferred $c$-axis orientation. Also vital (although not just from the neutron standpoint) is the fact that Grafoil can be baked in vacuum at high temperatures to remove impurities and, when fully outgassed, has surfaces of exceptional uniformity and homogeneity. This, of course, is why it is so useful for macroscopic adsorption studies.

In light of the forgoing discussion, it might be helpful to pause at this point and briefly consider how LEED and neutron diffraction compare as probes of surface films. One of the very considerable advantages of LEED is that there is little restriction on the choice of substrate. Almost any surface which can be prepared with single facet exposure and outgassed by electron bombardment under high vacuum is acceptable. Another valuable feature of LEED is that large specific areas are not needed. Both techniques are alike, however, in requiring a careful selection of gases for physisorbed studies; LEED because of desorption problems and neutron diffraction because of difficulties with background discrimination. Of course, for chemisorbed systems, where desorption and high vapor pressure do not present problems, LEED is almost universally applicable.

As we remarked earlier, an important advantage of neutrons is that they do not cause significant film evaporation and can therefore be used even with weakly bound surface layers. Furthermore, the higher vapor pressures associated with either higher temperatures, weakly bound films, or multilayer films do not interfere with neutron measurements. In fact, in contrast to LEED, which can only explore low converage films, neutron measurements become progressively easier as the number of surface layers increases because the scattered intensity is proportional to the total amount of adsorbed gas. Thus it is possible to study films from submonolayer coverages up to the bulk limit. And last but not least, it should be emphasized that in a few special cases neutrons have a potential for dynamic studies which exceeds the current LEED capability.[24]

On a purely practical level there are also points of difference between LEED and neutron methods which are worthy of comment. Because neutrons are very penetrating, samples for neutron investigations can be mounted in gas tight containers and located within thermally shielded environments such as cryostats and ovens without seriously interfering with experimental flexibility. Consequently, once outgassed and sealed, substrates for neutron spectroscopy can be recycled many times without further processing.

## III. EXPERIMENTAL APPARATUS AND PROCEDURES

### A. Sample preparation, gas handling, and thermometry

Our initial studies of surface monolayers involved nitrogen films adsorbed on Grafoil.[25] The adsorbent consisted of 60.5 g of stacked Grafoil disks forming a cylinder 4.4 cm high and 4.4 cm in diameter.[26] For faster equilibration, each disk was pierced with three 0.5-cm-diam holes to allow easier access of gas to the interior. A close fitting aluminum cell with walls 0.05 cm thick in the region traversed by the beam was used as the sample container. To remove contamination

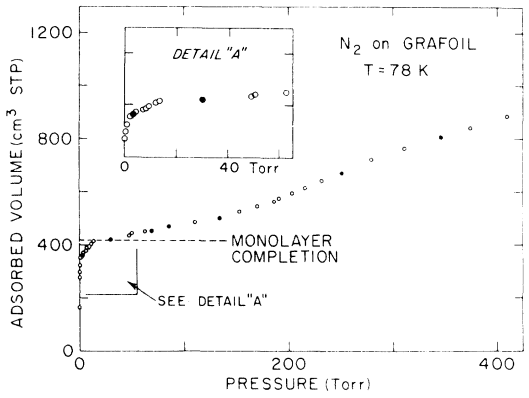


FIG. 1. Vapor-pressure isotherm at $T = 78$ K for the sample used in these measurements. The adsorbed volume has been corrected for dead volume in the cell. The solid circles identify the points at which the diffraction scans of Fig. 12 were made.

from the Grafoil surfaces, the disks were baked for 25 min at 1400 °C in an argon-filled furnace. When cool, they were removed from the furnace under an argon atmosphere and loaded into the cell which was then sealed with an indium O-ring. Access to the cell was provided through a valve mounted in its top.

Two methods were used to calibrate the effective surface area of the Grafoil: (i) $N_2$ adsorption isotherms, and (ii) determination of the quantity of gas required to form a complete, $\sqrt{3}\times\sqrt{3}$, registered phase. The $N_2$ isotherm measurement consisted of identifying the "knee" corresponding to completion of the first atomic layer and then computing the area of the layer as the measured quantity of gas multiplied by a standard $N_2$ molecular area factor—16.4 Å$^2$.[27,28] This is regarded as a reliable and consistent method for the comparison of different gases and substrates. It is believed to introduce an uncertainty of no more than 10–20% and to be reproducible to within narrower limits. $N_2$ adsorption isotherms for the sample used were measured independently at Brookhaven and at the University of Washington with the same result, which is shown in Fig. 1. Locating the knee of the isotherm at 415 cm$^3$, the adsorption area was found to be 1810 m$^2$ giving a specific area of 30 m$^2$/g.[26] This is in reasonable agreement with the value 1740 m$^2$ obtained by measuring the critical coverage and lattice constant of the registered phase (see Sec. IV C).

The sample cell was mounted in the tail section of a variable-temperature helium cryostat with access for the gas provided by a thin-walled Cu-Ni capillary.[29] Sample temperatures were measured with calibrated plantium and germanium resistance thermometers embedded in the aluminum container.

The amount of gas loaded into the cell for a given scan was determined from $P$-$V$-$T$ measurements made at room temperature using calibrated volumes and a precision capacitance pressure gauge. To maintain purity, condensible contaminants were removed from the gas by passing it through a baked 13X zeolite filter before introducing it into the system. Whenever the coverage was changed, the sample was warmed to at least 78 K to anneal and equilibrate the adsorbed film. Each time this was done, the vapor pressure was monitored to insure that the samples were fully equilibrated before the diffraction measurements began. For scans in which the temperature rather than the coverage was changed, we adjusted the total volume of gas in the system to maintain a constant quantity of gas in the adsorbed phase. In this case, adjustments for the amount of gas in the vapor phase were based on the known dead volumes (warm and cold[29]) and on the measured pressure in the system.

### B. Neutron spectroscopy

All diffraction scans were made with a conventional two-axis neutron spectrometer operated with a fixed neutron wavelength of 4.17 Å—a value chosen to optimize contrast between scattering from the adsorbed film and the substrate as was discussed in Sec. II. A curved pyrolytic graphite crystal was used as monochromator. High-order (shorter-wavelength) contamination was removed from the incident beam by passing it through a liquid-nitrogen-cooled, polycrystalline beryllium filter mounted in front of the monochromator. Horizontal beam divergence was restricted by Soller collimators to 40 min of arc in each of the three sections of the spectrometer.

Scans were always normalized to a fixed number of counts recorded by a stable, low-efficiency fission monitor mounted in the monochromatic beam in front of the sample. In every case the sample cell and cryostat were held in fixed position during the scan and only the scattering angle $2\theta$ was varied. While a few of the longest scans covered an angular range from 10 to 120 deg, most were restricted to the angular interval of primary interest between 55 and 90 deg. Counting times were typically 2 min/point. The solid line in Fig. 2 shows the results of a typical scan.

Background scattering from the Grafoil substrate and aluminum container, indicated by the dashed line in Fig. 2, was measured at temperatures of 20, 40, 60, and 80 K with the cell empty of gas. Over most of the angular range of interest, the background was featureless, except in the neighborhood of $2\theta = 77$–$78$ deg where a prominent peak coming from the graphite 002 reflection is evident. The 90-deg misorientation of crystallites responsible

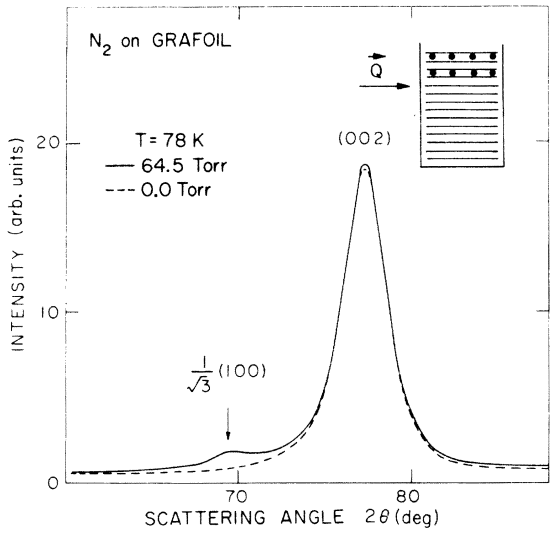


FIG. 2. Scattered neutron intensity from the sample cell at $T = 78$ K. The dashed curve is the background with no $N_2$ in the cell ($P = 0$ Torr) while the solid curve represents scattering with approximately 1.1 adsorbed layers ($P = 64.5$ Torr). The inset shows the scattering geometry used for all measurements with the neutron wave-vector transfer $\vec{Q}$ aligned parallel to the substrate foil plane.

for this peak is not believed to have resulted from the cutting and piercing of the foils during sample preparation but rather from the way in which the material was originally processed.[30]

In addition to the 002 peak, there was also a rising trend in the background at scattering angles smaller than those covered by Fig. 2. This scattering is thought to result from Fresnel diffraction by individual graphite crystallites but multiple Bragg scattering may also be in part responsible.

All of our diffraction profiles show excessive statistical scatter and systematic error in the neighborhood of $2\theta = 77$–$78$ deg. This difficulty, which will be further discussed in Sec. IV B 2 is due to the high background intensity from the 002 graphite reflection which makes the signal-to-background ratio poor in this general vicinity. Although unwanted, the 002 graphite peak did have some slight utility in that it served as a fiducial point for correction of individual scans for slight variations in the alignment of the neutron spectrometer arm.

Independent neutron rocking curve measurements were made on samples of the Grafoil we used. These established that the graphite crystallites were oriented in the foil with their $c$-axis distribution peaked normal to the macroscopic foil plane, i.e., with their basal planes preferentially oriented parallel to the plane of the foils. The full width at half-maximum of the $c$-axis distribution was observed to be about 30 deg. Since all scans were made with the axis of the sample cell normal to the plane of the spectrometer (see inset to Fig. 2), the graphite basal planes in the sample were therefore preferentially oriented parallel to the neutron scattering plane for all measurements.

## IV. DIFFRACTION FROM MONOLAYER FILMS

### A. Theory of 2D diffraction

von Laue[31] appears to have been the first to consider how radiation diffracts from 2D crystals. Following his original analysis, Warren,[32] Wilson,[33] Méring[34] and others developed detailed models of 2D diffraction which are now routinely used to analyze x-ray scattering from layered compounds. These models, described in textbooks concerned with the fundamentals of x-ray crystallography,[35] are equally applicable to neutron scattering. We will not attempt to reproduce them here. It will suffice for our purposes simply to summarize those results essential to the interpretation of our data. Readers not familiar with the subject will find a full discussion in Refs. 32–35 and related literature.

Before going into detail, however, it might be helpful to outline some of the basic features of diffraction from ordered layered materials. As will shortly become evident, there are two major factors which determine the shape of 2D profiles. First, as von Laue originally showed, the reciprocal lattice of a 2D crystal consists of an ordered array of rods, aligned normal to the crystal plane. In a sample of 2D crystallites randomly oriented in 3D space, this produces a diffracted line with a characteristic "sawtooth" shape, i.e., a line with a sharply rising leading edge on the low-angle side, followed by a trailing edge extending to larger scattering angles. Second, the shape of the trailing edge is substantially modified when (as is often the case) the 2D crystallites are not completely random in orientation. In this case the exact shape of the line will depend on the amount of preferred orientation and on how the sample itself is aligned with respect to the scattering plane.

#### *1. Diffraction from randomly oriented monolayers*

The conventional approach to 2D theory is to consider the coherent reflection of radiation from an assembly of planar arrays which are randomly oriented in 3D space, each array consisting of molecules or atoms arranged on a 2D lattice. Following Warren,[32] it can be shown that in this case the intensity diffracted by the $hk$th Bragg reflection is given by the following expression:

$$I_{hk} \propto N \frac{m_{hk} |F_{hk}|^2 f^2(\theta) e^{-2W}}{(\sin\theta)^{3/2}} \left(\frac{L}{\pi^{1/2}\lambda}\right)^{1/2} \mathcal{F}(a) , \quad (1)$$

where $2\theta$ is the scattering angle, $m_{hk}$ represents the multiplicity of the $hk$th reflection, $F_{hk}$ is the crystal structure factor, $f(\theta)$ the molecular form factor, and $e^{-2W}$ the 2D Debye-Waller factor. The other quantities in Eq. (1) are the wavelength $\lambda$, a parameter $L$ which Warren identified with the size of the 2D array, and

$$\mathcal{F}(a) \equiv \int_0^\infty e^{-(x^2-a)^2}\, dx \ ,$$

where $a = (2\pi^{1/2}L/\lambda)(\sin\theta - \sin\theta_{hk})$ and $\theta_{hk} = \sin^{-1}(\lambda/2d_{hk})$, $d_{hk}$ being the 2D plane spacing for the $hk$th reflection.

When $a$ is large, Eq. (1) reduces to the simpler and more often quoted form

$$I_{hk} \propto N \frac{m_{hk} F_{hk}^2 f^2(\theta) e^{-2W}}{\sin\theta(\sin^2\theta - \sin^2\theta_{hk})^{1/2}} \ . \qquad (2)$$

It is easy to see from these expressions that after an initial rise at $\theta_{hk}$, the intensity will decrease slowly at larger angles.

We will assume that molecular orientational ordering does not occur in the films we are investigating. In this circumstance, for small values of the scattering vector $\vec{Q}$, the molecular form factor in Eq. (1) or (2) takes the form[36]

$$f(\theta) = 2j_0(\tfrac{1}{2}Ql) \ , \qquad (3)$$

where $j_0$ is the zeroth-order spherical Bessel function, $|\vec{Q}| = 4\pi\sin\theta/\lambda$, and $l$ is the bond length in the molecule (1.1 Å for $N_2$ gas). In general $f^2(\theta)$ introduces an oscillatory modulation of the basic profile, but in our scans $\frac{1}{2}Ql < \pi$ and $f^2(\theta)$ consequently decreases monotonically over the angular range of interest.

### 2. *Influence of preferred 2D crystallite orientation*

Equation (1) presupposes an array of 2D crystallites with completely random orientation. In Grafoil, individual crystallites tend to align with their $c$ axes normal to the foil plane. We can take this into account by introducing into the analysis a function $H(\gamma)$ representing the probability that the plane of a given 2D crystallite is tilted at an angle $\gamma$ with respect to the foil plane. To generalize Eq. (1) we assume that $H(\gamma)$ can be expressed as the sum of two terms

$$H(\gamma) = H_0 + H_1 \exp[-\tfrac{1}{2}(\gamma/\delta)^2] \ , \qquad (4)$$

the first representing the purely random part of the distribution and the second an oriented component with an effective mosaic parameter $\delta$. $H(\gamma)$ is normalized by requiring that $\int_0^{\pi} H(\gamma)\, d\gamma \equiv 1$. Expression (4) then defines the distribution of crystallites in the foils in terms of two parameters; $H_0/H_1$, which characterizes the ratio of random to oriented crystallite planes, and $\delta$, the width of the oriented part of the distribution.

To relate the polar angle $\gamma$ to the scattering angle $2\theta$, we note that the condition for Bragg reflection from a 2D crystal is that the scattering vector $\vec{Q}$ terminates on a reciprocal lattice rod. It is easy to see from Fig. 3 that for a given value of $\vec{Q}$ lying in the foil plane, only 2D crystals oriented in such a way that $\gamma = \cos^{-1}(\sin\theta_{hk}/\sin\theta)$ can contribute to the Bragg reflected intensity. Thus $I_{hk}$ as given by Eq. (1) is weighted by a factor $H[\cos^{-1}(\sin\theta_{hk}/\sin\theta)]$ to account for the effects of preferred orientation. From this it follows that when the most probable orientation of the 2D planes is parallel to the scattering vector, scattering is shifted into the angular region near $2\theta_{hk}$ at the expense of scattering at larger angles, i.e., the profiles become more symmetric and more like those observed in 3D diffraction.

### 3. *Diffraction from multilayers*

As additional layers are condensed on top of the surface monolayer, the 2D, sawtooth diffraction profiles are gradually transformed into symmetric, 3D powder lines. The transformation is produced by interference effects. Instead of uniform intensity along the 2D Bragg rods, regions of high intensity develop at the points which will become Bragg points in the 3D reciprocal lattice. Ultimately, the scattering is entirely concentrated at these points and the diffraction becomes fully three dimensional.

Interference effects enter the 2D theory through the structure factor

$$F_{hk} = \sum_{j=1}^{n} b_j \exp\{-i[2\pi(hx_j + ky_j) + cQ_\perp z_j)]\} \ , \qquad (5)$$

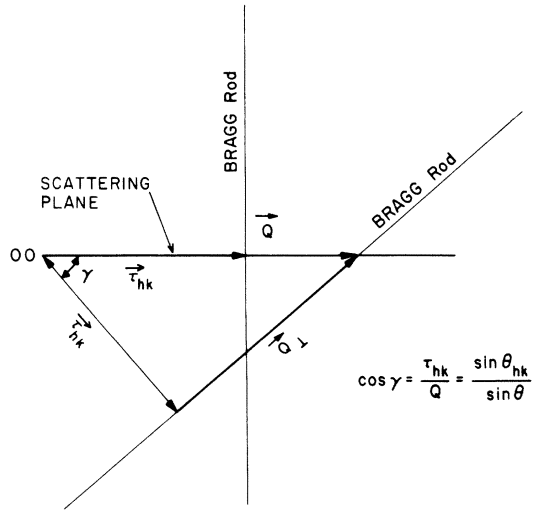


FIG. 3. Scattering diagram in reciprocal space for a pair of 2-D polycrystals; one oriented parallel to the neutron scattering plane and the other tilted at an angle $\gamma$.

in which $b_j$ represents the coherent scattering amplitude of the $j$th atom in the unit cell, $x_j$, $y_j$, and $z_j$ are its reduced positional coordinates, $c$ is the interlayer spacing, and $Q_\perp$ defines the component of the scattering vector normal to the 2D lattice plane (as shown in Fig. 3). The summation extends over all atoms in the unit cell. Formulated in this way, the theory treats multilayer films as though they were two dimensional, but it is the 3D unit cells which form a 2D lattice.

To obtain a quantitative picture of how the added layers influence the scattering, let us consider a specific example of practical interest, namely the scattering from two layers of identical atoms arranged in an ordered lattice. For the sake of generality, we suppose that the second layer is incomplete and that it contains some fraction $f$ of the number of atoms in the first layer. Assuming the scattering from the two layer regions to be independent of the scattering from the monolayer regions, we find from Eq. (5)

$$|F_{hk}(Q_\perp)|^2 = b^2\{1+f+2f\cos[2\pi(hx_2+ky_2) + cQ_\perp z_2]\} . \tag{6}$$

With multilayer films, it is particularly important to determine to what extent the diffracted line shapes reflect the details of the structure of the two layer parts of the film. This point is best investigated by examining the form of $F^2_{hk}$ for specific examples. For the sake of simplicity let us restrict our consideration to the 10 Bragg reflection which, in our present case, is the only one accessible to experimental investigation because of the long wavelength employed. Two representative ordered arrangements of the adsorbed layers come immediately to mind: (a) a second layer with atoms located directly over those in the first layer, and (b) a second layer with atoms sited at the centers of the equilateral triangles formed by the atoms in the first layer lattice.[21] For the first case, $x_2 = y_2 = 0$, $z_2 = 1$, and

$$|F_{\{10\}}(Q_\perp)|^2 = b^2(1+f+2f\cos cQ_\perp) . \tag{7a}$$

For the second case, $x_2 = \frac{1}{3}$, $y_2 = \frac{2}{3}$, $z_2 = 1$, and

$$|F_{\{10\}}(Q_\perp)|^2 = b^2(1+f-f\cos cQ_\perp) . \tag{7b}$$

(The symbol $\{10\}$ indicates an average over the 10 and 01 reflections.) One can see simply from inspection that expressions (7a) and (7b) will lead to significantly different diffraction profiles.

For the sake of completeness we should also consider a third alternative arrangement of the two layers, namely that each layer remains ordered within itself but there is only partial registry between the layers. In this case the structure factor will take the form

$$|F_{hk}(Q_\perp)|^2 = b^2\{1+f+2f[\langle\cos 2\pi(hx_2+ky_2)\rangle \times \cos cQ_\perp + \langle\sin 2\pi(hx_2+ky_2)\rangle \operatorname{sinc} cQ_\perp]\} , \tag{7c}$$

where the angular brackets indicate an average over all unit cells. Of course, when there is no registry at all between the two layers, then $\langle\cos 2\pi(hx_2+ky_2)\rangle = \langle\sin 2\pi(hx_2+ky_2)\rangle = 0$ (unless $h=k=0$) and $F^2_{hk}(Q_\perp) = (1+f)b^2$, i.e., the two layers scatter incoherently.

### B. Comparison of 2D diffraction theory with experiment

Before proceeding further, it will be valuable to see how well the observed line shapes compare with the diffraction profiles predicted by our 2D model. As we have been at pains to make clear, such a comparison involves a detailed understanding of the relationship between the 2D character of the diffracting films and the shape of the diffraction profiles. It will also, however, require that the effects of instrumental resolution be taken properly into account.

Since complete treatments of instrumental resolution in two-axis neutron spectrometers are available in the literature,[37] there is no need for us to go into detail here. It will suffice to say that the instrumental line profile can be approximated by a Gaussian resolution function of the form

$$R(\theta) = (1/\Delta\pi^{1/2})\exp(-\theta/\Delta)^2 , \tag{8}$$

the width parameter $\Delta$ being determined by the spectrometer collimation and the monochromator plane spacing. In a diffraction scan, we can expect to observe the convolution of $R(\theta)$ with the ideal line profile, i.e., with $H(\gamma)I_{hk}(\theta)$, as defined above. In other words, the observed angular variation of intensity can be expected to be of the form

$$g_{hk}(\theta) = \int R(\theta-\theta')\,H(\gamma)I_{hk}(\theta')\,d\theta' . \tag{9}$$

Section V will be devoted to a discussion of the various diffraction profiles which appear at different film coverages and temperatures. Here, for purposes of making detailed comparisons with diffraction theory, let us concentrate our attention on two representative scans made under conditions in which the structure of the films is reasonably easy to define.

#### *1. Registered phase monolayer*

Our first example is a low-temperature scan of diffraction from 400 $cm^3$ STP of adsorbed $N_2$, an essentially complete monolayer as determined from the isotherm of Fig. 1. Plotted in Fig. 4 as the solid circles is the observed scattering from the 10 Bragg reflection. Also plotted is a solid

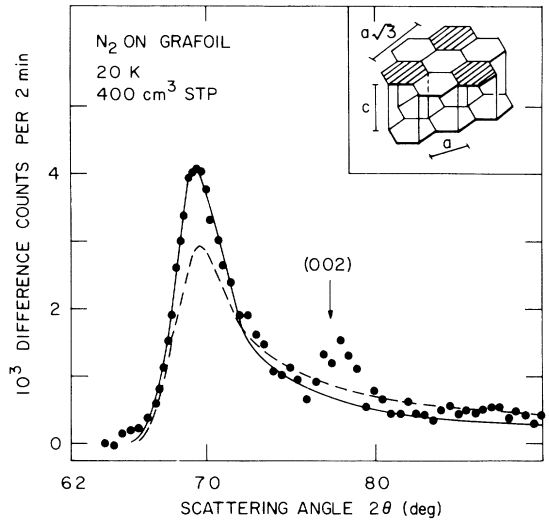


FIG. 4. Diffraction profile at $T = 20$ K of the 10 Bragg reflection from a monolayer of $N_2$ in $\sqrt{3}\times\sqrt{3}$ registry on the Grafoil substrate. Background scattering with no $N_2$ in the cell has been subtracted. The solid curve was calculated using Eq. (9) with orientation parameters $H_0/H_1 = 0.78$ and $\delta = 12.7°$. The dashed curve indicates the line shape expected with random orientation of the substrate crystallites. The peak near $2\theta = 77°$ is related to the background from the 002 graphite reflection as discussed in the text. Illustrated in the inset is the $\sqrt{3}\times\sqrt{3}$ lattice in registry on the graphite basal plane.

line showing the excellent fit to the data obtained using Eq. (9) with $I_{hk}$ as defined by Eq. (1) and $H(\gamma)$ as defined by Eq. (4). The values used for the orientation parameters $H_0/H_1$ and $\delta$ are given in the figure caption. In computing this curve, the Debye-Waller factor was arbitrarily set equal to unity, the bond length $l$ was taken to be 1.1 Å and $\Delta$, the effective resolution of the spectrometer, was assigned the value $0.5/2(\ln 2)^{1/2}$ corresponding to the measured instrumental full width at half-maximum (in terms of $\theta$) of 0.5 deg of arc. The other required quantities, i.e., the array size $L$, the 2D plane spacing $d_{10}$ and the sample orientation parameters $H_0/H_1$ and $\delta$ were regarded as parameters of the fit. Although it may not be obvious from casual inspection, $L$ is effectively defined by the leading edge of the line while the product $e^{-2W}H(\gamma)$ is fixed by the intensity profile of the trailing edge.[38] The value obtained for $L$ was 105 Å, indicative of the effective size of the 2D crystallites responsible for the scattering.

It is interesting to note that by using the Scherrer formula $L_c = \lambda/\beta\cos\theta$ (where $\beta$ is the *fwhm* of the unfolded line) we obtain from the width of the 002 graphite peak in Fig. 2 a value of 107 Å for $L_c$, the thickness in the $c$-axis direction of the 90-deg misoriented graphite crystallites. Thus it appears that the disoriented crystallites, which provide the larger part of the surface area in Grafoil, have thicknesses comparable to their breadths. This probably explains why they do not assume a preferred orientation.

As would intuitively be expected, the 2D plane spacing is essentially determined by the position of the diffraction peak. From the data of Fig. 4 a value of 3.678 Å is obtained for $d_{10}$. Assuming a triangular lattice, this value implies a nearest-neighbor distance $a_{nn}$ of 4.247 Å, which is within 0.3% of 4.259 Å,[39] the *nn* distance expected in the $\sqrt{3}\times\sqrt{3}$ epitaxial phase illustrated in the inset to the figure. Thus the implication is strong that the $N_2$ film is in registry on the graphite basal planes.[40] Further support for this interpretation comes from the fact that a careful search failed to reveal any of the additional diffraction peaks expected for other ordered 2D structures.

Also included in the figure as a matter of interest is the line shape predicted for a randomly oriented array of 2D crystallites. This is the dashed curve. Comparison of the solid and dashed curves shows how preferred $c$-axis orientation in Grafoil enhances the scattering in the vicinity of the diffraction peak.

### 2. *Dense phase bilayer*

As a second example, let us consider the low-temperature scan shown in Fig. 5 which is the diffraction pattern observed with 800 $cm^3$ STP of adsorbed $N_2$ in the cell—an almost complete two-

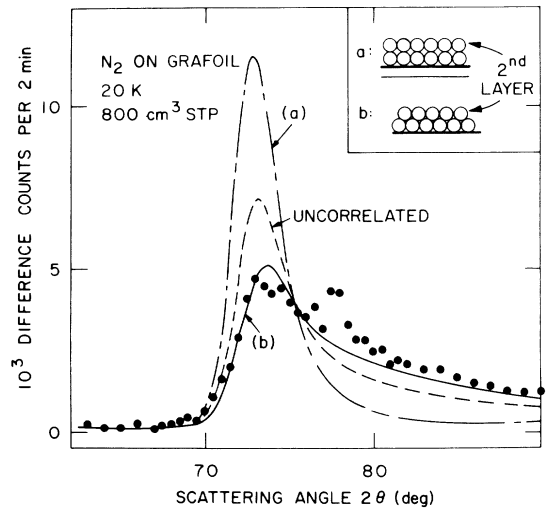


FIG. 5. Diffraction profile at $T = 20$ K of the 10 Bragg reflection from the dense phase bilayer. The calculated line shapes shown are for the two packing arrangements illustrated and for identical ordered layers with no positional correlation. The peak near $2\theta = 77°$ is related to the large background from the 002 graphite peak as discussed in the text.

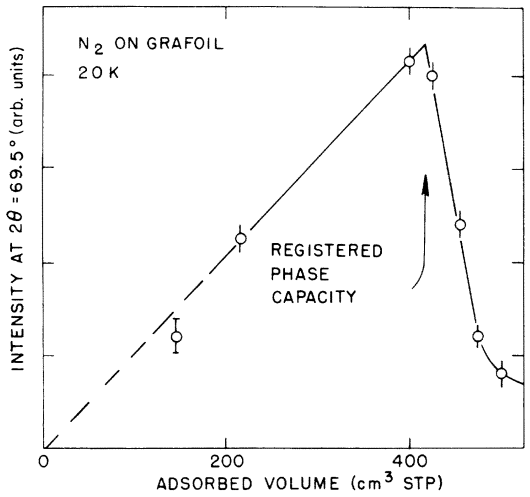


FIG. 6. Intensity of the $\sqrt{3}\times\sqrt{3}$ registered phase diffraction peak ($2\theta = 69.5°$) as a function of coverage at $T = 20$ K.

layer film. The dash-dotted curve plotted in the figure represents the line shape predicted assuming two-layer configuration (a) as illustrated in the inset to the figure, the solid curve was calculated assuming configuration, (b) while the dashed curve indicates the profile expected if there is no positional correlation between the layers. All curves were computed using the array size and substrate orientation parameters obtained from the monolayer data of Fig. 4 and with the Debye-Waller factor set equal to unity. The over-all normalization was, however, scaled to match the larger quantity of adsorbed gas. For the curves of Fig. 5, an isotropic background was assumed, its value estimated from the scattering near $2\theta = 55$ deg. As explained in Sec. IV A 3 above, differences in the configuration of the two layers were introduced into the computation through the assumed form of the structure factor, i.e., by using either Eq. (7a), (7b), or (7c). Only the distance $c$ between the layers[41] and the plane spacing $d_{10}$ were left as parameters to be determined by fitting to the data. As is apparent from Fig. 5, the close packed structure defined by Eq. (7b) gives the best fit to the data.

A point of particular interest in the scan of Fig. 5 is the outward shift in the position of the diffraction peak which indicates that the presence of the second layer has produced considerable lateral compression of the film. Assuming once again a triangular lattice, the *nn* distance is in this case found to be 4.037 Å, some 4% smaller than $a_{nn}$ for the registered phase. There will be more examples of this so-called "dense phase" in the scans to follow.

A further point concerning not only the above mentioned scans but all others as well is that the peak which appears at $2\theta = 78$ deg results from imperfect subtraction of the background scattering in the vicinity of the 002 graphite reflection. We suspect that it occurs because the adsorbed film slightly enhances the intensity of the 002 reflection. If so, it indicates that the gas layers form at approximately the graphite interplanar distance above the substrate surface. We hasten to add, however, that there may be other more mundane explanations for the effect.

### C. Surface-area calibration

Earlier we mentioned that the registered phase scattering could be used to make an independent determination of the surface area of the Grafoil substrate. Figure 6 illustrates how this was done. In it we show the variation with coverage of the intensity of scattering from the registered phase (at a temperature of 20 K). A sharp break at 415 $cm^3$ STP is evident. This we interpret as indicating complete coverage of all accessible basal plane surfaces with a monolayer of registered phase film. Knowing the lattice constant of the registered phase lattice (and from this the area per $N_2$ molecule), and assuming all the gas is present as a registered phase, it is then easy to deduce that 415 $cm^3$ of gas corresponds to a surface area of 1740 $m^2$, the value quoted in Sec. III A.

## V. EXPERIMENTAL RESULTS

The discussion in the previous section was intended to indicate the extent to which the observed line shapes can be correlated with the predictions of 2D diffraction theory and to illustrate the methods available to us to define the characteristics of the adsorbed films and the Grafoil substrate. With these ideas in mind let us now turn our attention to the diffraction patterns observed at other coverages and temperatures.

Altogether we investigated a number of film coverages in the range between $\frac{1}{3}$ and $1\frac{3}{4}$ layers at temperatures from 10 to 90 K. Figure 7 shows the coverages and temperatures at which individual scans were made. In general, as the coverage and temperature were varied the diffraction patterns also changed. In some cases, such as those discussed earlier, the profiles could be related with reasonable confidence to particular states of the surface film; in others, for reasons which will become clear at a later stage, we were not able to define the structure of the film in an unambiguous way from the observed line shapes.

At coverages below one monolayer and at high temperatures, the diffraction patterns are broad and poorly defined indicative of a phase in which the range of order is very limited. Figure 8(a) shows an example of the profile observed at a

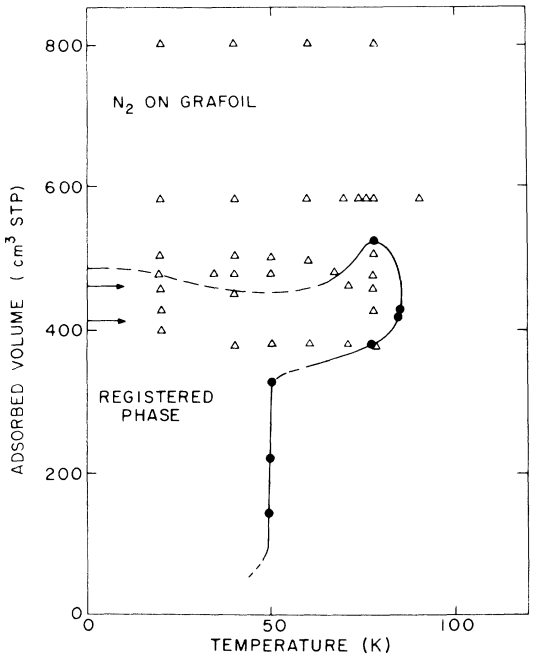


FIG. 7. Plot indicating the temperatures and coverages where extended diffraction scans were made (Δ) and where transitions involving the $\sqrt{3}\times\sqrt{3}$ registered phase were observed (●). The arrows indicate the monolayer capacity of the registered phase and the dense phase at 415 $cm^3$ STP and 460 $cm^3$ STP, respectively. $\sqrt{3}\times\sqrt{3}$ registered phase is observed everywhere within the curved boundary.

temperature of 78 K with 360 $cm^3$ STP of $N_2$ on on the substrate, i.e., 0.87 of a monolayer of registered phase. Upon lowering the temperature to 70 K with the coverage held constant, a peak develops at $2\theta = 69.5$ deg, the scattering angle of the registered phase. This is shown in Fig. 8(b). Further cooling causes the registered phase scattering to increase rapidly at the expense of scattering from the disordered phase. Ultimately, at a temperature of about 50 K the scattering saturates as is evident in Figs. 8(c) and 8(d). It is clear that the registered phase is the stable low-temperature configuration at this coverage. (In this and the following figures the solid lines represent fits to the Warren model and will be discussed in Sec. VI.)

The above behavior is characteristic of coverages between roughly 350 and 400 $cm^3$ STP. At lower coverages, however, the broad distributions of Fig. 8(a) persist down to a temperature of about 50 K at which point the diffraction profile changes over a temperature range of only a few degrees to the familiar registered phase form.

When the coverage is raised above the registered phase limit of 415 $cm^3$, the situation alters. This is illustrated in Fig. 9 which shows how the diffraction profiles change as the coverage is increased from 400 to 800 $cm^3$ with the temperature held constant at 20 K, i.e., it shows how the registered phase monolayer line shape of Fig. 4 evolves into the dense phase, bilayer line shape of Fig. 5. We note that at 455 $cm^3$ the peak has shifted from its registered phase position to a larger scattering angle, the leading edge of the line has broadened

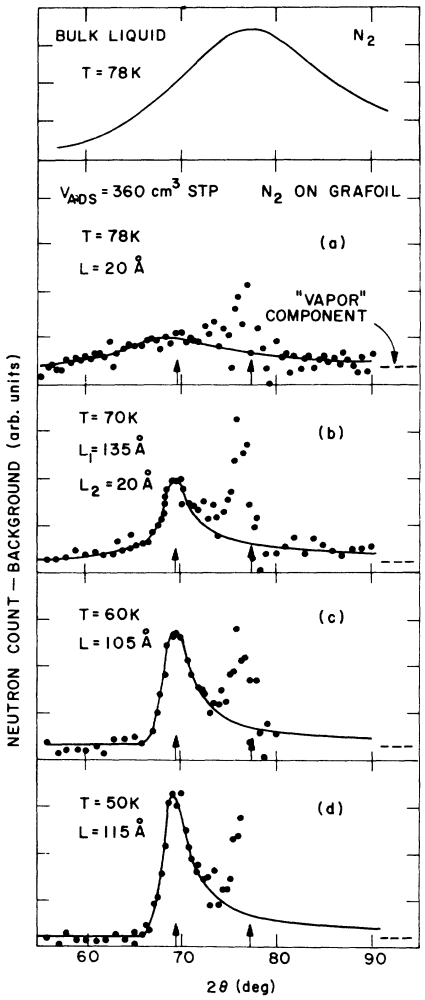


FIG. 8. Temperature dependence of the diffraction observed with an adsorbed volume of 360 $cm^3$ STP (0.87 layers). The solid curves are line shapes calculated from Eq. (9) with orientation parameters $H_0/H_1 = 0.78$ and $\delta = 12.7°$. A constant "vapor" contribution to the scattering (indicated by the dashed line) was assumed for each scan. The scan at 70 K was fitted by assuming it to be a composite of the scans at 78 and 50 K, i.e., assuming it to be scattering from a mixture of disordered and $\sqrt{3}\times\sqrt{3}$ registered phases. The arrows indicate the peak position corresponding to a nearest-neighbor distance $a_{nn} = 4.25$ Å and the position of the 002 graphite reflection ($2\theta = 77.3°$). The solid curve at the top of the figure represents scattering from bulk liquid nitrogen at 78 K observed under identical experimental conditions.

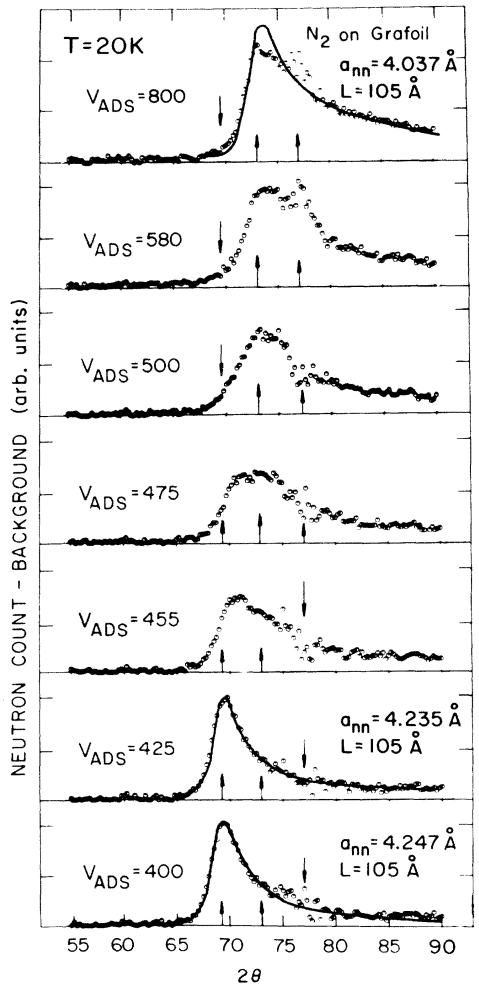


FIG. 9. Diffraction profiles observed at 20 K with adsorbed volumes ranging from 400 to 800 cm$^3$ STP. The solid curves for 400, 425, and 800 cm$^3$ represent best fits to Eq. (9) with orientation parameters $H_0/H_1 = 0.78$ and $\delta = 12.7°$. The arrows indicate the peak positions at the two extremes of coverage and the position of the 002 reflection from the graphite substrate.

and the trailing edge has flattened. When the coverage is increased to 500 cm$^3$ the peak position is that of the dense phase but the leading edge of the line remains noticably broadened. Finally when 800 cm$^3$ of $N_2$ is on the surface the leading edge of the line narrows and the profile assumes the dense phase bilayer form.

As we remarked in Sec. IV B 2, the *nn* distance in the dense phase is some 4% too small for simple registry. Nevertheless, partial registry (every *n*th molecule at the center of a basal plane hexagon) remains a possibility. But if a superlattice actually formed in the dense phase, new diffraction peaks could be expected to show up at smaller scattering angles. Since no evidence of satellite reflections was found in any of our low-angle data, it would appear that the dense phase, although ordered, is not in registry on the basal plane surfaces.

In Fig. 10 we show a scan sequence made with a fixed coverage of 475 cm$^3$ over the temperature range from 10 to 78 K. At temperatures below 30 K the film is evidently in the dense phase as judged by the position of the peak, but the leading edge of the line is broadened. Above 30 K both the leading and trailing edges of the line become sharper although the film remains nominally in the dense phase. Finally, at a temperature below 50 K rapid expansion begins as indicated by the shift to smaller angles in the position of the peak. At 78 K the expansion terminates with the formation of a registered phase. The registered phase persists to 84.5 K (although it is not evident from the figure) and then the diffraction

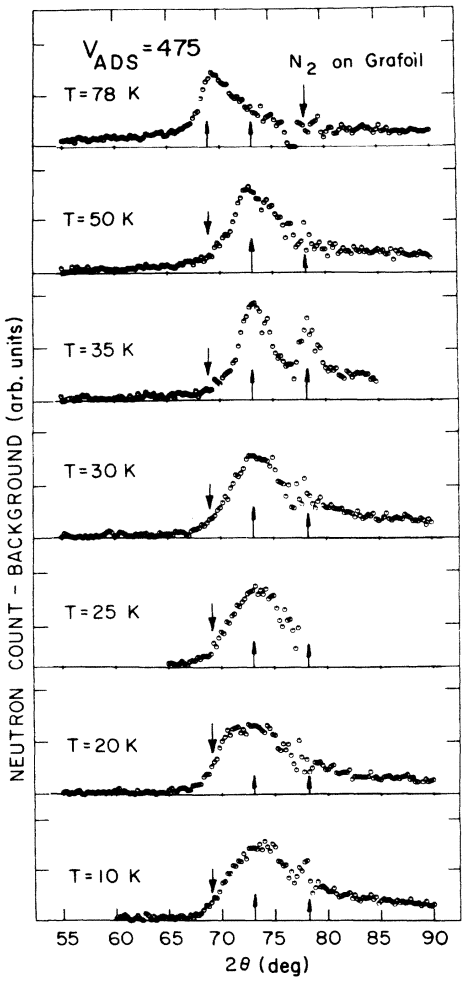


FIG. 10. Temperature dependence of the diffraction with 475 cm$^3$ STP of $N_2$ adsorbed on the Grafoil substrate. The arrows indicate the peak positions for the $\sqrt{3}\times\sqrt{3}$ registered phase, the dense phase and the 002 reflection from the graphite substrate.

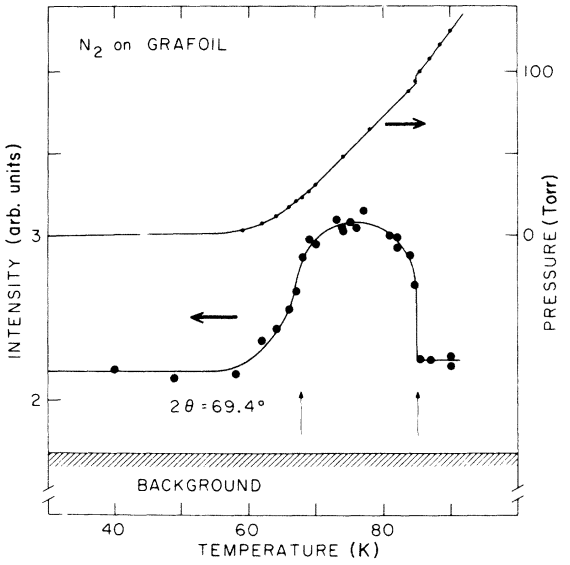


FIG. 11. The temperature dependence of the neutron intensity at the $\sqrt{3}\times\sqrt{3}$ registered phase peak ($2\theta = 69.4°$) and the corresponding vapor pressure in the sample cell. The adsorbed volume on the substrate varied from 460 $cm^3$ STP at $T = 40$ K to 415 $cm^3$ STP at $T = 85$ K. The neutron intensity is proportional to the number of molecules in the registered phase.

pattern abruptly broadens indicating a transition to a disordered phase.

This rather complicated sequence of transitions can perhaps be best appreciated by noting how the intensity of scattering from the registered phase varies over the temperature range under consideration. This is shown in Fig. 11 where we have also plotted as a matter of interest the vapor pressure above the adsorbed film surface. Note that there is a discontinuous change in the vapor pressure at 84.5 K, the temperature of the registered phase-disordered phase transition. We should mention that the measurements shown in this figure were made with a fixed total amount of gas in the sample cell. As a consequence, the quantity of $N_2$ on the Grafoil surface varied from about 460 $cm^3$ at temperatures below 60 K to roughly 415 $cm^3$ at 85 K.

It is also interesting and a little surprising to see that at higher temperatures the registered phase persists at coverages above 415 $cm^3$. This is illustrated in Fig. 12 where it is evident that at 78 K the registered phase is stable even with 500 $cm^3$ of $N_2$ on the substrate surface. We should also call attention to the fact that when the coverage increases beyond 500 $cm^3$ the line broadens considerably and at the same time the diffraction peak shifts towards the dense phase position.

From Fig. 12 we can also see that the changes in the slope of the adsorption isotherm of Fig. 1 correlate with the changes observed in the diffraction patterns. For example, the break at 360 $cm^3$ seems to be identified with the first appearance of the registered phase—the completion of this phase being indicated by an abrupt decrease in slope at 415 $cm^3$. In the neighborhood of 520 $cm^3$ there is an increase in slope. This we can see from our diffraction data to be the point at which the surface film has been forced completely out of registry.

The scans in Figs. 13 and 14 show the temperature dependence of the dense phase diffraction profiles at coverages of 580 and 800 $cm^3$, respectively. At the lower coverage of Fig. 13 the film expands readily, as judged by the inward shift in the position of the peak with increasing temperature, while at the higher coverage of Fig. 14, which represents nearly two complete dense layers, the film becomes noticeably stiffer. The solid lines in the two figures represent fits to the Warren model discussed in Sec. IV and will be discussed in detail in Sec. VI.

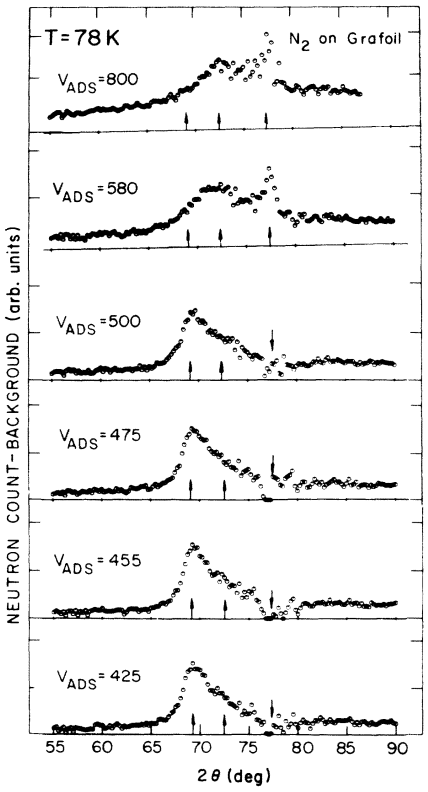


FIG. 12. Diffraction profiles observed for a number of coverages along the adsorption isotherm at $T = 78$ K (see Fig. 1). The arrows indicate the peak positions of the registered and dense phases and the position of the 002 reflection from the graphite substrate.

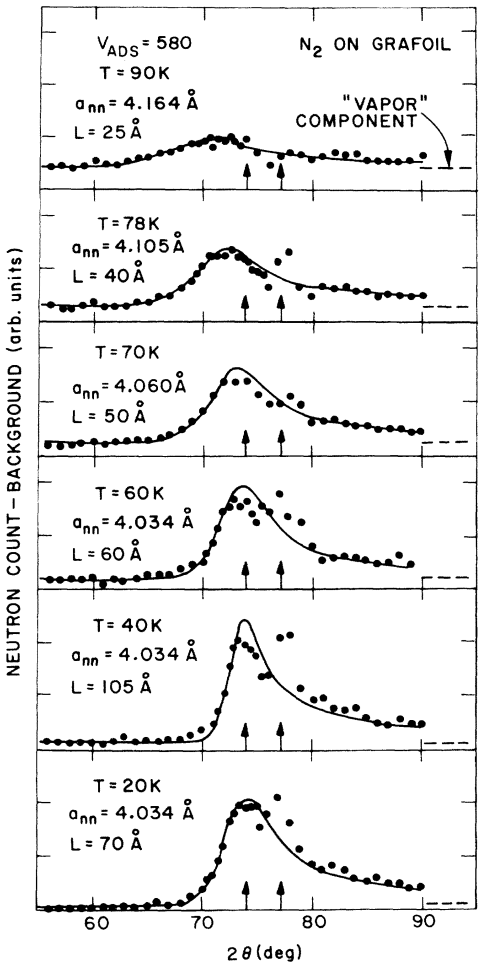


FIG. 13. Temperature dependence of the diffraction scans at an adsorbed volume of 580 $cm^3$ STP. The solid curves are best fits to Eq. (9) with orientation parameters $H_0/H_1 = 0.78$ and $\delta = 12.7°$. In each scan an isotropic "vapor component" was assumed as indicated by the dashed line. For the scans at $T = 20$ and 40 K the one-fourth complete top layer was assumed to have close-packed positional correlation with the bottom layer. For the higher-temperature scans it was necessary to assume the top layer uncorrelated with the bottom layer to fit the data. The arrows indicate the peak position at the lowest temperature and the position of the 002 reflection from the graphite substrate.

## VI. ANALYSIS OF DATA

In Sec. IV we showed that the 2D diffraction profiles from *single phases* could be analyzed to determine the nearest-neighbor distance in the film, the size of the diffracting array and, in multiple layer films, the degree and type of registry between layers. With *coexisting phases*, however, the situation is less straightforward although it is at least clear that the existence of mixed phases can be detected by the composite character of the diffraction patterns they produce. But determining the properties of the phases involved or in some cases even identifying them can be difficult, particularly if nearly identical structures are involved. Of course when the phases are quite different in character their contributions to the scattering are more easily separated. Thus the 70 K scan of Fig. 8 representing scattering from a mixture of ordered and disordered phases could be decomposed with reasonable confidence into separate components while few of the scans in Figs. 9, 10, and 12, which appear to involve a mixture of dense and registered phases, could be similarly resolved.

As a general principle, whenever we were rea-

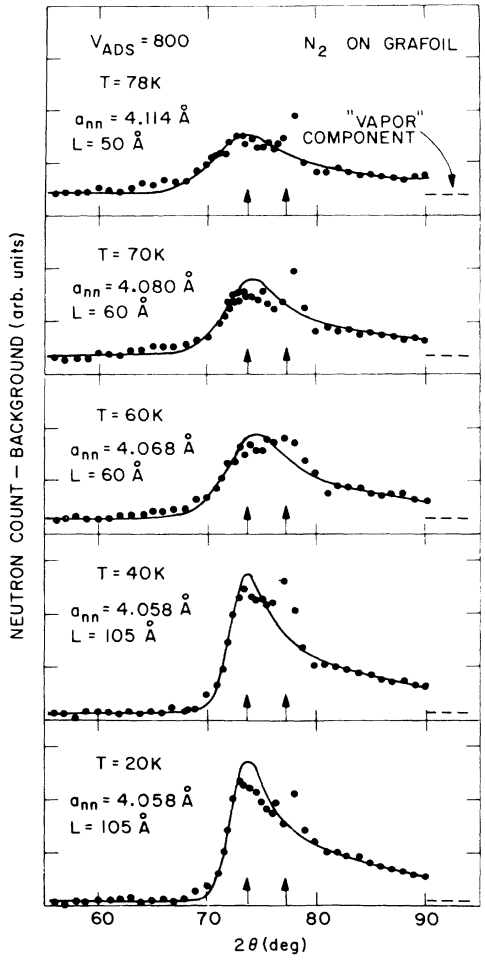


FIG. 14. Temperature dependence of the diffraction scans at an adsorbed volume of 800 $cm^3$ STP. The solid curves represent best fits to Eq. (9) with orientation parameters $H_0/H_1 = 0.78$ and $\delta = 12.7°$. At all temperatures the three-quarter complete top layer was assumed to have close-packed positional correlation with the bottom layer. The arrows indicate the peak position at the lowest temperature and the position of the 002 reflection from the graphite substrate.

sonably certain that we were either dealing with a single phase or could divide the observed scattering into contributions from individual phases, we attempted to extract from the data values for the 2D plane spacing $d_{10}$ and the line width parameter $L$, which Warren equates with the size of the 2D crystallites. Since we find $L$ to decrease at higher temperatures, we prefer to think of it as defining the range of spatial correlations in the film rather than the size of the diffracting arrays. In this regard it should also be mentioned that the range of order in idealized 2D systems and its variation with temperature are subjects of considerable theoretical interest. Calculations made by Imry and Gunther[42] indicate that when fluctuations are included the Warren model for the line shape is not completely correct as far as the details of the leading edge are concerned. But the differences are subtle and probably beyond the limits of our current sensitivity and in any case we are not certain of the extent to which adsorbed $N_2$ films ought to be regarded as idealized 2D structures. Consequently we have not attempted to extend our analysis beyond the simple Warren model.

It ought also to be remarked that the fits we have obtained to the diffraction patterns are not necessarily unique. In our fitting procedure we assumed, for reasons of simplicity, that no molecular ordering took place and that the Debye-Waller factor was unity. But it should be emphasized that both these assumptions primarily influence the fit to the trailing edge of the line and have little effect on the determination of either the linewidth parameter $L$ or the 2D plane spacing $d_{10}$.

Because of problems in identifying the phases involved, only the data of Figs. 8, 13, and 14 and the two lowest coverage scans in Fig. 9 were analyzed in detail. In Fig. 8 the sequence of scans shows how the diffraction patterns change as the system evolves from a low-temperature registered phase to a mixed phase and ultimately to a disordered phase at the highest temperature. The solid lines represent best fits of Eq. (9) to the data with $a_{nn} = 4.25$ Å and values of $L$ as indicated. It is important to note that we found it necessary to assume coexistence of the high-temperature disordered phase with the low-temperature registered phase to obtain a satisfactory fit to the 70-K data.

On the basis of the diffraction data alone, there is no way to decide whether the disordered monolayer phase observed at 78 K is a 2D liquid or an amorphous solid. It is evident, however, that the disordered phase diffraction peak occurs at the registered phase position and is shifted some 7.1 deg inward from that of bulk liquid nitrogen observed under identical conditions (see solid curve at top of Fig. 8). Thus $a_{nn}$ in the 2D disordered phase is 4.25 Å, significantly larger than the value 4.0 Å obtained for the bulk liquid.[43] Although disordered, the $N_2$ molecules in this phase nevertheless appear to be constrained to epitaxy by the periodic potential of the graphite substrate.

Turning now to the data of Figs. 13 and 14, we considered these scans to represent dense phase, partial bilayer films. The proportion of $N_2$ present as a second layer was estimated by calculating the volume of gas necessary to produce a complete monolayer of dense phase and assuming the remaining gas was adsorbed on top of this layer. In the case of the lower coverage data of Fig. 13 we estimated that $\frac{1}{4}$ of a second layer was present, while for the higher-coverage data of Fig. 14 the second layer was estimated to be $\frac{3}{4}$ complete. It was assumed that the same value of $L$ could be assigned to each layer and that (with the exception of temperatures above 40 K for the 580-cm$^3$ coverage) the second layer formed in registry on top of the first layer as described in Sec. IV B 2.

The solid lines in Figs. 13 and 14 represent best fits of Eq. (9) to the data with fitting parameters $a_{nn}$ and $L$ as indicated. Figure 15 shows the temperature dependence of these quantities. Note

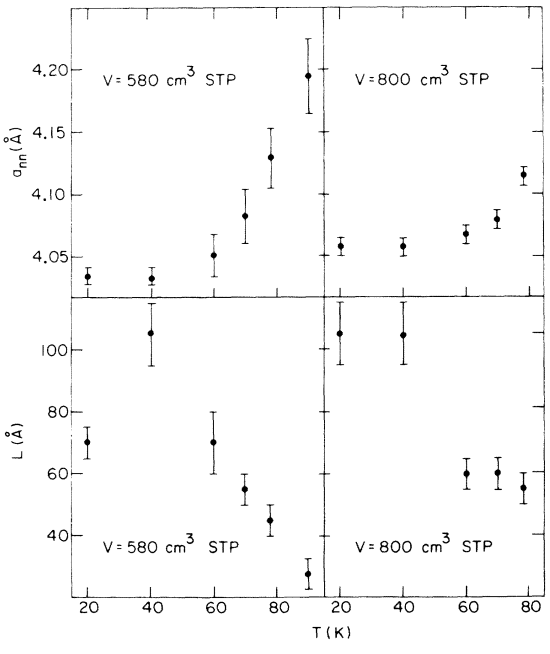


FIG. 15. Temperature dependence of the nearest-neighbor distance $a_{nn}$ and the positional correlation range $L$ for the data of Figs. 13 and 14. The error limits at high temperatures for $V = 580$ cm$^3$/STP were estimated by calculating the line shapes with varying degrees of correlation between the first and second layers. In general, the uncertainties increase at higher temperatures due to broadening of the diffraction peaks.

that for the lower-coverage film the nearest-neighbor distance increases about 2.5% between 20 and 78 K while for the higher coverage film $a_{nn}$ increases only 1.4% over the same temperature range. Apparently increasing the amount of second layer improves the stability of the film as is also evident from the fact that the range of correlation in the higher-coverage film can be seen to decrease less rapidly with increasing temperature. (The drop in $L$ for the lower-coverage film at the lowest temperature should probably not be attributed to a decrease in the range of correlation but rather to the fact that part of the film has formed a registered phase.)

Expansion and decreasing order are not the only changes which occur in dense phase films as they get warmer. Also to be noted in Figs. 13 and 14, and in fact in Fig. 8 as well, is the rise in isotropic scattering with increasing temperature which is particularly noticeable at the smaller angles. This very likely originates from the "vapor" component of the surface layer which evidently increases at the expense of the "solid" component as the temperature gets higher. Another curious feature of the data plotted in Fig. 14 is the appearance on the low-angle side of the diffraction peaks of a small contribution to the scattering from a disordered phase. This shows up first in the scan at 60 K and persists at higher temperatures. It may indicate the presence of liquid component, but this cannot be established with any certainty from the diffraction data.

Finally, before leaving the subject of data analysis, we would like to comment on Bourdon, Marti, and Thorel's alternative explanation[44] of what we have referred to as "dense phase" diffraction profiles. They suggest that these profiles result from diffraction by a close-packed registered phase in which the axes of the $N_2$ molecules are tilted at an angle of 67 deg relative to the normal to the film plane. We question the viability of this explanation for two reasons. First, argon is known to form a nonregistered phase on graphite at submonolayer coverages[21] and in this case there can be no possibility of other interpretations of the data involving orientational ordering. So the existence of nonregistered phases on graphite seems beyond question. Second, the smooth and continuous change of lattice constant with temperature shown in Fig. 15 is not easily explained on the basis of a registered phase model but is easy to reconcile with the existence of a nonregistered phase.

## VII. DISCUSSION

Our diffraction studies indicate that at low temperatures monolayers of $N_2$ adsorbed on Grafoil form one of two recognizably different phases depending on the coverage. Of these, the low-coverage, registered phase evidently has true long-range positional order since the molecules locate themselves at the centers of the graphite basal plane hexagons. Except near monolayer coverages, transitions from this phase to the disordered, high-temperature phase seem to be first-order processes involving a discontinuous change in the crystallographic order. The other phase, the dense phase associated with higher coverages, appears to be of different character. As evidence of this we note the marked variation with temperature of the positions and widths of the diffraction peaks indicating that this phase, in contrast to the registered phase, is not positionally constrained by the underlying substrate structure. Also, in the dense phase, the transition from an ordered system at low temperatures to a disordered one at high temperatures seems to be a continuous rather than a discontinuous process. There is thus the implication that the dense phase is a system without true long-range order even at the lowest temperatures. This is of course suggestive of an idealized, 2D solid which, according to theory,[45] is only fully positionally ordered in the zero-temperature limit.

At high temperatures, the data indicate that adsorbed $N_2$ films exist as a disordered phase. Unfortunately, it is impossible to tell from the diffraction patterns alone whether the phase is a liquid or an amorphous solid. Specific-heat measurements of $^4$He monolayers on Grafoil,[7,8] which have been interpreted in terms of a continuous melting process, support the view but do not prove that it is a liquid phase we are observing. Our results would have been more definitive in this regard if we could have energy analyzed the scattered neutron beam. We did in fact attempt this but the intensities were not sufficient to allow any clear cut conclusions.

On the basis of this study as well as investigations made by others of the thermodynamic properties of gases adsorbed on graphite, we are emboldened to propose a tentative phase diagram for the *first* layer of $N_2$ on Grafoil. This diagram, shown in Fig. 16, is based on the corresponding 3D constant-volume phase diagram. We emphasize that only those phase boundaries appearing as solid lines in the figure have been established by our measurements. The dashed lines represent inferences from other measurements as well as a certain amount of educated guesswork on our part. What we understand to be unique about 2D-like systems is the existence of solid phases without true long-range positional order, i.e., phases which transform continuously, either by melting or layer promotion, from a solid to a disordered (liquid?) state. In this sense, the registered

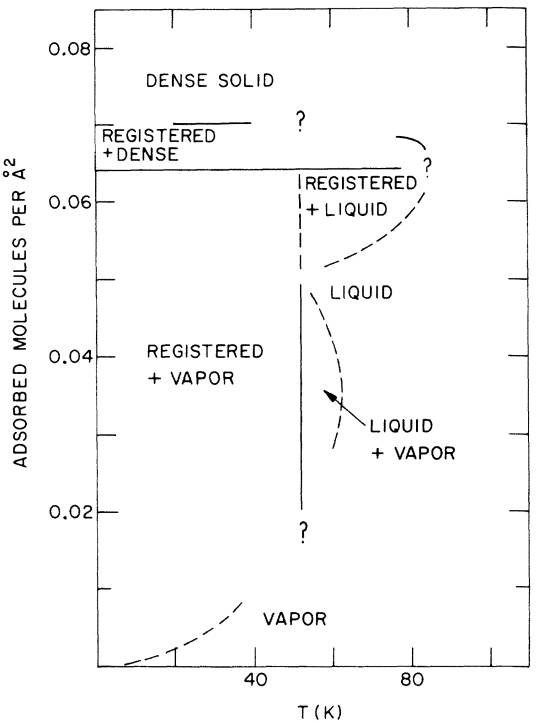


FIG. 16. Proposed phase diagram for the *first* layer of $N_2$ adsorbed on Grafoil. Constant coverage scans do not necessarily represent constant areal density contours on the figure because of film expansion and layer promotion as discussed in the text.

phase which appears at low coverages cannot be strictly regarded as a 2D phase since it has the imposed spatial order of the substrate.

In interpreting Fig. 16 it is important to keep in mind that constant coverage scans do not necessarily represent constant areal density contours on the phase diagram. This is in part because the dense phase films expand with increasing temperature and in part because layer promotion depletes the surface monolayer. A striking illustration of this appears in the highest-temperature scan of Fig. 10 where the surface monolayer has evidently been sufficiently depleted to cause a transition from the dense to the registered phase.

It is not altogether clear in fact that the dense phase exists as a monolayer film. If we define the effective surface area in terms of the registered phase coverage (as discussed in Sec. IV C) then we can estimate from the dense phase lattice constant that 460 $cm^3$ of $N_2$ is necessary to form a complete dense phase monolayer. But the low-temperature scans of Fig. 10 indicate a mixture of registered and dense phases even with 475 $cm^3$ in the cell. Thus there is reason to suspect that the more dense packing of the film is linked to the formation of a second layer. If so, a word of caution is in order; the dense phase of nitrogen adsorbed on Grafoil, which we are tempted to regard as a 2D system, may not ever exist as a 2D structure.

In closing, we would like to emphasize once again that analysis of our low-temperature diffraction data indicates that multilayer $N_2$ films have the same close packed structure as the 3D solid. At higher temperatures the range of positional correlation in these films diminishes as is evident in Figs. 13 and 14 and the degree of registry between layers presumably weakens. Although we have not shown the data, ultimately, at temperatures on the order of 90 K, the observed diffraction profiles from adsorbed phases (at least at high coverages) become indistinguishable from those of the bulk liquid.

## ACKNOWLEDGMENTS

We are obligated to Dr. Y. Imry for clarifying a number of points concerning the theory of idealized 2D systems. Also we wish to express our thanks to Dr. K. Carneiro for help in compiling the table of neutron cross sections and for a careful review of the manuscript, to T. Chung for assistance in preparing the sample, and to Dr. M. B. Dowell for supplying us with high-purity Grafoil for our investigations.

*Work performed under the auspices of the U. S. Energy Research and development Agency.

†Present address: Research Establishment Risø, *DK* 4000 Roskilde, Denmark.

[1]A discussion of the limitations of 2D models of absorbed films is given by A. D. Novaco, in *Monolayer and Submonolayer Films*, edited by J. G. Daunt and E. Lerner (Plenum, New York, 1973), p. 75.

[2]M. H. Polley, W. D. Schaeffer, and W. R. Smith, J. Phys. Chem. 57, 469 (1953).

[3]J. H. Singleton and G. D. Halsey, Jr., J. Phys. Chem. 58, 330 (1954); 58, 1011 (1954).

[4]B. B. Fisher and W. G. McMillan, J. Am. Chem. Soc. 79, 2969 (1957).

[5]T. Takaishi and M. Saito, J. Phys. Chem. 71, 453 (1967).

[6]Y. Larher, J. Phys. Chem. 72, 1847 (1968); and J. Colloid Interface Sci. 37, 836 (1971).

[7]A. Thomy and X. Duval, J. Chem. Phys. Physicochim. Biol. 66, 1966 (1969); 67, 286 (1970); 67, 1101 (1970).

[8]M. Bretz, J. G. Dash, D. C. Hickernell, E. O. McLean, and O. E. Vilches, Phys. Rev. A 8, 1589 (1973); A 9, 2814(E) (1974).

[9]R. L. Elgin and D. L. Goodstein, Phys. Rev. A 9, 2657 (1974).

[10]Grafoil is the trade name of a product marketed by the Union Carbide Corp., Carbon Products Div., 270 Park Ave., New York, N. Y.

[11]D. F. Brewer, A. Evenson, and A. L. Thomson, J. Low Temp. Phys. 3, 603 (1970).

[12]W. A. Steele and R. Karl, J. Colloid Interface Sci. 28, 397 (1968).

[13]A. A. Antoniou, P. H. Scaife, and J. M. Peacock, J. Chem. Phys. 54, 5403 (1971).
[14]G. B. Huff and J. G. Dash, in *Proceedings of the 13th International Conference on Low Temperature Physics*, edited by K. D. Timmerhaus, W. J. O'Sullivan, and E. F. Hammel (Plenum, New York, 1974).
[15]J. J. Lander and J. Morrison, Surf. Sci. 6, 1 (1967).
[16]J. Suzanne, J. P. Coulomb, and M. Bienfait, Surf. Sci. 40, 414 (1973).
[17]P. W. Palmberg, Surf. Sci. 25, 598 (1971).
[18]H. H. Farrell, M. Strongin, and J. M. Dickey, Phys. Rev. B 6, 4703 (1972).
[19]H. Saltsburg, in *Monolayer and Submonolayer Helium Films*, edited by J. G. Daunt and E. Lerner (Plenum, New York, 1973), p. 149.
[20]E. W. Plummer, *Monolayer and Submonolayer Helium Films*, edited by J. G. Daunt and E. Lerner (Plenum, New York, 1973), p. 157.
[21]H. Taub, L. Passell, J. K. Kjems, K. Carneiro, J. P. McTague, and J. G. Dash, Phys. Rev. Lett. 34, 654 (1975).
[22]J. K. Kjems, L. Passell, H. Taub, and J. G. Dash, Phys. Rev. Lett. 32, 724 (1974).
[23]At the relatively small momentum transfers typical of this measurement, diatomic molecules act more or less like point scatterers. In the low-momentum limit the scattering cross section of a molecule becomes simply $4\pi(\sum_j b_j)^2$, where the $b_j$'s represent the scattering amplitudes of the constituent atoms. The next to last column in Table I indicates the influence of the molecular form factor $j_0(\frac{1}{2}Ql)$ on the cross section at a momentum transfer corresponding to $\sqrt{3}\times\sqrt{3}$ registered phase on graphite.
[24]J. P. Coulomb, J. Suzanne, M. Bienfait, and P. Masri, Solid State Commun. 15, 1585 (1974); J. P. Coulomb and P. Masri, *ibid.* 15, 1623 (1974).
[25]E. Lerner and J. G. Daunt [J. Low Temp. Phys. 10, 299 (1973)] have studied some of the bulk thermodynamic properties of this system.
[26]In Ref. 21 the total number of foils in the sample cell was incorrectly stated as 317. The correct number is approximately 115. The isotherms and other parameters of the cell are unchanged by this error. It also has no effect on any of the quoted properties of the films or on our conclusions.
[27]D. M. Young and A. D. Crowell, *Physical Adsorption of Gases* (Butterworths, London, 1962).
[28]W. D. McCormick, D. L. Goodstein, and J. G. Dash, Phys. Rev. 168, 249 (1968).
[29]Dead volume in the sample cell and capillary was estimated on the basis of room-temperature gas displacement to be about 20 $cm^3$ out of a total volume of 80 $cm^3$.
[30]M. B. Dowell (private communication).
[31]M. von Laue, Z. Kristallogr. 82, 127 (1932).
[32]B. E. Warren, Phys. Rev. 59, 693 (1941). Equation (1) in the text is basically Eq. (39) in this paper. The structure factor, molecular form factor and Debye-Waller factor were added to make it applicable to the case we are discussing.
[33]A. J. C. Wilson, Acta Crystallogr. 2, 245 (1949).
[34]P. J. Méring, Acta Crystallogr. 2, 371 (1949).
[35]See, for example, L. V. Azaroff, *Elements of X-Ray Crystallography* (McGraw-Hill, New York, 1968), Chap. 10.
[36]V. F. Sears, Can. J. Phys. 44, 1279 (1966); 44, 1299 (1966).
[37]M. J. Cooper and R. Nathans, Acta Crystallogr. A 24, 619 (1968).
[38]The intensity distribution in the trailing edge of the diffraction profile determines the produce $e^{-2W}H(\gamma)$, not $H(\gamma)$ alone. With only the 10 diffraction peak accessible, we have no way of independently determining the Debye-Waller factor. If we arbitrarily set $2W=0$, as we have done, then the 2D array orientation as defined by $H_0/H_1$ and $\delta$ implies *less* preferred orientation than is indicated by the rocking curve measured for the 002 reflection from the graphite substrate (a conclusion which is *not* altered by assuming a finite value for $2W$). Since the 002 rocking curve is actually a measure of the mosaic distribution of the 002 planes rather than of the adsorption surfaces, we conclude that most of the gas is adsorbed on the smaller graphite crystallites, with less preferred orientation. These presumably have a larger area-to-volume ratio than the larger crystallites which produce the bulk of the 002 diffraction.
[39]Y. Baskin and L. Meyer, Phys. Rev. 100, 544 (1955).
[40]Xe adsorbed on graphite has also been observed to form a registered phase as reported in Refs. 15 and 16. Indirect evidence of a registered phase has also been obtained from bulk measurements of $^3$He and $^4$He adsorbed on Grafoil as reported in Refs. 8 and 9.
[41]Although 2D diffraction profiles are very sensitive to the $x$ and $y$ coordinates of the second layer, they are relatively unaffected by changes in the assumed interplanar distance $c$. The computations of Fig. 5 were made with $c=3.3$ Å, however, any value within 20% of this would have fitted the data equally well.
[42]Y. Imry and L. Gunther, Phys. Rev. B 3, 3939 (1971).
[43]J. H. Clark, J. C. Dowe, and R. N. Sinclair, Mol. Phys. 29, 581 (1975).
[44]A. Bourdon, C. Marti, and P. Thorel, Phys. Rev. Lett. 35, 544 (1974).
[45]N. N. Bogoliubov, Phys. Abh. Sowjetunion 6, 113 (1962).